

# Adaptive-optics performance of Antarctic telescopes

Jon S. Lawrence

The performance of natural guide star adaptive-optics systems for telescopes located on the Antarctic plateau is evaluated and compared with adaptive-optics systems operated with the characteristic mid-latitude atmosphere found at Mauna Kea. A 2-m telescope with tip-tilt correction and an 8-m telescope equipped with a high-order adaptive-optics system are considered. Because of the large isoplanatic angle of the South Pole atmosphere, the anisoplanatic error associated with an adaptive-optics correction is negligible, and the achievable resolution is determined only by the fitting error associated with the number of corrected wave-front modes, which depends on the number of actuators on the deformable mirror. The usable field of view of an adaptive-optics equipped Antarctic telescope is thus orders of magnitude larger than for a similar telescope located at a mid-latitude site; this large field of view obviates the necessity for multiconjugate adaptive-optics systems that use multiple laser guide stars. These results, combined with the low infrared sky backgrounds, indicate that the Antarctic plateau is the best site on Earth at which to perform high-resolution imaging with large telescopes, either over large fields of view or with appreciable sky coverage. Preliminary site-testing results obtained recently from the Dome Concordia station indicate that this site is far superior to even the South Pole. © 2004 Optical Society of America

*OCIS codes:* 010.1080, 010.1330, 350.1260, 350.1270.

## 1. Introduction

Degradation of resolution caused by atmospheric turbulence is detrimental to any astronomical observation from a ground-based site. The use of adaptive-optics systems to alleviate this problem on small to large telescopes is becoming increasingly reliable and has allowed the generation of astronomical images whose resolution approaches the diffraction limit.<sup>1,2</sup> However, the small field of view over which adaptive-optics systems are typically efficient is a serious limitation on the applicability of these systems, and existing solutions to these problems are technologically challenging.<sup>3</sup> In this paper the performance of an adaptive-optics system on telescopes located on the Antarctic plateau, where the unique atmospheric characteristics indicate that wide-field-of-view imaging with high-order adaptive optics systems should be possible, is analyzed.

An astronomical adaptive-optics system works to correct the turbulence-induced atmospheric phase

distortion by measuring the distortion introduced on a reference source (the guide star) with a wave-front sensor. A deformable mirror (for high-order correction) or a tiltable mirror (for low-order tip-tilt correction) or both are then used to remove this distortion from the wave front that originates from the object to be imaged. Limitation in the degree of correction achievable arises from errors introduced throughout the system; the most significant for field-of-view considerations is known as anisoplanatic error. This error occurs because the light from the guide star and the light from the object to be imaged traverse different paths through the atmosphere owing to the angular separation of the reference and the object star. Thus the atmospheric phase distortion experienced by each optical path is different. There is also an opposed error term that is due to the signal-to-noise ratio (SNR) associated with the wave-front measurement. This error increases for smaller separation angles because brighter stars are more difficult to find. Techniques to reduce these errors include the use of multiple guide stars, the use of laser guide stars or beacons,<sup>4</sup> and the use of multiple deformable mirrors matched to separate atmospheric layers (multiconjugate adaptive optics<sup>5</sup>). There are, however, disadvantages to each of these techniques. Multiple natural guide stars do increase the useful field of view, but not significantly. Laser guide star systems necessitate the use of specialized laser sys-

---

The author (jl@phys.unsw.edu.au) is with the School of Physics, University of New South Wales, Sydney, New South Wales 2052, Australia.

Received 1 July 2003; revised manuscript received 14 October 2003; accepted 17 October 2003.

0003-6935/04/061435-15\$15.00/0

© 2004 Optical Society of America

tems and require a natural guide star for tip-tilt correction. Multiconjugate adaptive optics systems have the potential to increase the usable field of view dramatically; however, they require complicated and expensive systems.

A parameter often used as an indication of the anisoplanatic error for a particular site is the isoplanatic patch or angle. It is defined in various ways<sup>6</sup> but generally represents the angular field of view over which an adaptive-optics system will correct the atmospheric distortion to a particular resolution (usually defined as the Strehl ratio). The Strehl ratio depends on the observation wavelength, the zenith angle, and the refractive-index structure constant profile of the atmosphere above any particular site. The isoplanatic angle is a useful indicator of the relative performance of different sites, but many other factors must be considered if one is to evaluate the overall performance of an adaptive-optics system. Site-testing data have indicated that the isoplanatic angle observed at the South Pole is significantly larger<sup>7</sup> than those found at temperate latitude sites, such as La Palma, Cerro Paranal, and Mauna Kea.<sup>8</sup> This implies that anisoplanatic errors for telescopes equipped with adaptive-optics systems will be significantly fewer in Antarctica than at any other ground-based site.

An extensive site-testing campaign conducted over the past decade has shown that the Antarctic plateau is one of the best sites on Earth for performing infrared and submillimeter astronomy (see, for example, Refs. 9 and 10). First, because of low atmospheric temperatures, the sky's spectral brightness in the mid- and near-infrared is lower by as much as 2 orders of magnitude than the sky's spectral brightness that is typically observed at mid-latitude sites.<sup>11,12</sup> This significantly increases the sensitivity of any telescope located in Antarctica. Second, the low water-vapor content of the Antarctic atmosphere results in an increased atmospheric transmission and allows observations to be made at many infrared and submillimeter windows that are unobservable from other sites.<sup>13</sup> Third, the atmospheric turbulence above the Antarctic plateau has a unique profile that is not observed elsewhere. Although the ground-level seeing is only mediocre (1.8 arc sec at 0.5  $\mu\text{m}$ ) compared with that at the best mid-latitude sites, the majority of the atmospheric turbulence is confined to a layer within several hundreds of meters of ground level, and there is no high-altitude jet stream.<sup>7,14</sup> These conditions result in the large isoplanatic angle mentioned above.

Three Antarctic sites are considered to have atmospheric conditions that make them appropriate sites at which to locate an infrared telescope. The first site, the Amudsen-Scott U.S. South Pole station (0 °E, 0 °S, 2700-m elevation), is where the majority of site testing has taken place. This is a winter-capable station that currently has the logistic support necessary for operating an astronomical observatory. Currently, three submillimeter telescopes are operated throughout the Antarctic winter.<sup>15</sup> Previously

a prototype 600-mm infrared telescope, the South Pole Infrared Explorer<sup>16</sup> (SPIREX), equipped with a tip-tilt secondary mirror, had been successfully operated. The second site is Dome Concordia (Dome C; 123 °E, 75 °S, 3200-m elevation), where an Italian-French station is currently under construction for winter-over operation. Limited site-testing data have so far been obtained, but the higher elevation and the topography of the surrounding terrain indicate that this site will probably be superior for astronomy to the South Pole site.<sup>17</sup> An 800-mm infrared telescope [the Italian Robotic Antarctic Infrared Telescope (IRAiT)] is currently under construction for deployment in 2005 at Dome C. The third potential Antarctic astronomical site is Dome Argos (Dome A; 74 °E, 81 °S, 4200-m elevation). No site-testing data have yet been obtained from Dome A. However, owing to its location high on the Antarctic plateau, this site is potentially superior to both the South Pole site and Dome C. No station currently exists or is planned for Dome A, so the development of an observatory is only a long-term prospect.

It is assumed that the first stage in the development of an infrared observatory on the Antarctic plateau will consist of the design and construction of a small telescope with an  $\sim 2$ -m mirror diameter. A number of proposals to develop such an instrument currently exist; the proposed instruments include the Douglas Mawson Telescope (an Australian-French-Italian-U.S. collaboration) and the Arctic Infrared Laboratory (AIRO, a U.S. proposal). The primary role of such a telescope would be to perform sky surveys in the near to mid-infrared and to act as a test bed for future larger telescopes. As such, the adaptive optics system considered for the 2-m telescope consists only of a tip-tilt secondary mirror. The next generation of Antarctic telescopes is expected to be of considerable size (6–10 m) and to be equipped with a high-order adaptive optics system to utilize the advantageous aspects of atmospheric turbulence. A previous analysis of adaptive-optics performance for a South Pole telescope based on isoplanatic angle and integrated seeing has been published.<sup>18</sup> In this paper an analysis of the expected performance of adaptive-optics systems based on modeled turbulence profiles for an Antarctic atmosphere is compared with a standard model of the Mauna Kea atmosphere. Additionally, a first-generation 2-m and a second-generation 8-m telescope are considered.

## 2. Turbulent Structure

The spatial statistics that describe deformations in an optical wave front caused by propagation through a randomly inhomogeneous medium (the turbulent atmosphere) can be described by a quantity called the phase-structure function, defined by

$$D_{\phi}(r) = \langle [\phi(x+r) - \phi(x)]^2 \rangle, \quad (1)$$

which represents the phase variance between two points separated by a distance  $r$ . This wave-front phase variance is due to refractive-index variations

that can similarly be described by a refractive-index structure function,  $C_N^2$ , that are caused by temperature variations (described by a temperature structure function). The phase-structure function at the entrance of a telescope for Kolmogorov turbulence is described by<sup>19</sup>

$$D_\phi(r) = 6.88(r/r_0)^{5/3}, \quad (2)$$

where  $r_0$  is Fried's parameter, which represents the atmospheric coherence length. There are upper and lower bounds to the spatial scales over which Eq. (2) is valid. The following analysis thus holds only for an atmosphere with an inner turbulent scale that is much smaller than the telescope's diameter and an outer turbulent scale that is larger than the telescope's diameter. The first condition is considered acceptable, as the inner scale is typically a few millimeters.<sup>20</sup> The second condition is frequently used but sometimes disputed,<sup>21</sup> as measured values of the outer scale range from several meters to several tens of meters.<sup>22</sup> Fried's parameter<sup>23</sup> is given by

$$r_0 = 0.185\lambda^{6/5} \left\{ \sec(\theta) \int_0^\infty C_N^2(z) dz \right\}^{-3/5}, \quad (3)$$

where  $z$  is the height above ground level,  $\lambda$  is the observation wavelength, and  $\theta$  is the zenith angle of observation. It is an important parameter that is generally used to describe the spatial resolution capabilities of a particular site and is related to the full width at half-maximum (FWHM) of the seeing disk (for an infinitely large telescope) by<sup>24</sup>

$$\varphi_{\text{FWHM}} = 0.98(\lambda/r_0). \quad (4)$$

For a telescope equipped with any sort of adaptive-optics correction, however, the value of  $r_0$  alone is not a good indicator of the actual site quality.

To model the performance of an adaptive-optics system and make comparisons among different sites, atmospheric refractive-index structure constant profiles and horizontal wind speed profiles are required.

For the Mauna Kea (MK) atmosphere an analytic expression for the  $C_N^2$  profile, based on the Hufnagel-Valley boundary model,<sup>25</sup> is used. This general model has been derived from numerical values of  $C_N^2$  determined from microthermal balloon launches. It is given in the literature in various forms and with various coefficients (see, e.g., Refs. 26–28).  $C_N^2(z)$  is assigned a sum of exponential decays with increasing height  $z$  (above ground level) that is due to the main turbulent components of the atmosphere: a surface boundary layer (at  $\sim 3000$  m), a strong layer caused by the high-altitude jet stream (at  $\sim 6500$  m), and a (background) tropopause layer. The form used here is

$$C_N^2(z) = a_1 \exp\left(\frac{-z}{s_1}\right) + a_2 \exp\left[\frac{-(z-s_2)^2}{2d^2}\right] + a_3 \left(\frac{z}{s_3}\right)^{10} \exp\left(\frac{-z}{s_3}\right), \quad (5)$$

**Table 1.** Values of Coefficients Used in SP, SP25, and MK Atmospheric Models: Eqs. (5)–(7)

Coefficient	SP	SP25	MK
$a_1$ ( $\text{m}^{-2/3}$ )	$7.1 \times 10^{-15}$	$5.6 \times 10^{-15}$	$1.0 \times 10^{-17}$
$a_2$ ( $\text{m}^{-2/3}$ )	$5 \times 10^{-16}$	$1 \times 10^{-17}$	$5.0 \times 10^{-17}$
$a_3$ ( $\text{m}^{-2/3}$ )	$1 \times 10^{-17}$	$1 \times 10^{-18}$	$1.0 \times 10^{-40}$
$s_1$ (m)	70	40	3000
$s_2$ (m)	200	180	6500
$S_3$ (m)	500	400	1000
$d$ (m)	100	70	1000
$V_1$ ( $\text{m s}^{-1}$ )	5	3	6
$V_2$ ( $\text{m s}^{-1}$ )	11	6	30
$Z_1$ (m)	5000	5000	10000
$Z_2$ (m)	2600	2000	5000

where the coefficients are given in Table 1. They have been normalized to give  $r_0 = 0.15$  m at  $0.55 \mu\text{m}$  and an isoplanatic angle of 2 arc sec, representing typical seeing conditions at MK. The  $C_N^2$  function is shown in Fig. 1. The MK horizontal wind speed profile is given by the standard Bufton model<sup>26,29</sup>:

$$V_w^2(z) = v_1^2 + \left\{ v_2 \exp\left[\frac{-(z-z_1)}{2z_2^2}\right] \right\}^2, \quad (6)$$

which has the form of a Gaussian that comprises a ground wind speed component of  $6 \text{ m s}^{-2}$  and a high-altitude component that is due to the tropopause jet stream. The MK wind speed profile is shown in Fig. 2. Coefficients are given in Table 1.

An analytic form for the South Pole (SP) refractive-index structure constant profile is obtained from curve fits to data taken from the 2001 operation of the sonic detection and ranging (SODAR) instrumentation at the SP station<sup>14</sup> and from 1999 microthermal balloon launches that have been correlated with temperature gradients taken from meteorological balloon launches.<sup>7,30,31</sup> It is given a modified version of the Hufnagel-Valley boundary model,<sup>27</sup> with contributions<sup>32</sup> from a strong layer close to the ground (70 m) and a lower (200-m) and an upper (500-m) boundary layer:

$$C_N^2(z) = a_1 \exp\left[\frac{-(z-s_1)^2}{d^2}\right] + a_2 \exp\left(\frac{-z}{s_2}\right) + a_3 \exp\left(\frac{-z}{s_3}\right). \quad (7)$$

Values for the coefficients used in Eq. (7) are listed in Table 1, and the profile is shown in Fig. 1. The unique character of the Antarctic turbulence profile is apparent in the figure. Because of the lack of a high-altitude jet stream above the Antarctic continent, the nature of the katabatic winds that flow from higher up on the continent, and the extremely flat ground profile, the turbulence is confined within a layer that is on average only 300 m thick above the ice level.

Although the SODAR and balloon data derive  $C_N^2$  profiles only up to a distance of 1 km, comparisons with seeing data taken from the Antarctic Differen-

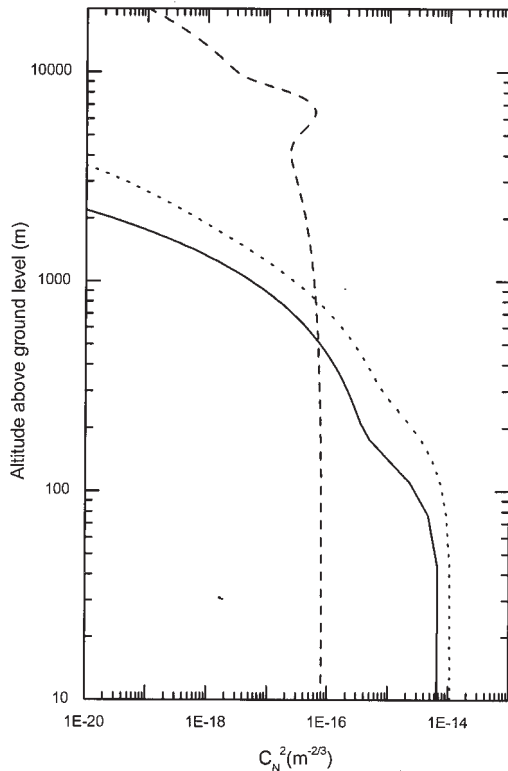


Fig. 1. Refractive-index structure constant ( $C_N^2$ ) profiles for the MK median (dotted curve), the SP median (dashed curve), and the SP25 (solid curve) atmospheres. The MK atmosphere is from the Hufnagel–Valley boundary model. The SP curves are from analytical fits of microthermal balloon and SODAR data.

tial Image Motion Monitor (ADIMM) confirm that the upper atmosphere's contribution (above the boundary layer) is negligible (it contributes less than 2% to the total seeing).<sup>32</sup> The coefficients used in Eq. (7) were fitted to average  $C_N^2$  profiles, and the upper-atmosphere component is then normalized to give a median ground-level coherence length of  $r_0 = 0.06$  m (at  $0.5 \mu\text{m}$ ), corresponding to a seeing FWHM of  $\sim 1.8''$ . To determine the effects of varying atmospheric conditions a model for the 25% best-seeing conditions at the South Pole (SP25) is also used. Statistical averages of SODAR, ADIMM, and microthermal balloon launch data give values for the best 25% seeing of  $r_0 \sim 0.099$  m ( $1.0''$ ) at  $0.5 \mu\text{m}$ .<sup>7,14,30</sup> Coefficients for the  $C_N^2$  profile normalized to give an  $r_0$  equal to these values are used to derive an estimate of the performance of the adaptive-optics system under the best atmospheric conditions. The 25% best  $C_N^2$  profile (SP25) is shown in Fig. 1, and coefficients are given in Table 1.

Meteorological balloon launches (recording temperature, pressure, and wind velocity) have been regularly made throughout the SP winter for the past decade. Four months of balloon data in the 2001 winter have been fitted to the Gaussian of the form in Eq. (6) for the median and 25% best values of the horizontal wind speed profiles. The profiles are shown in Fig. 2, and the coefficients are listed in

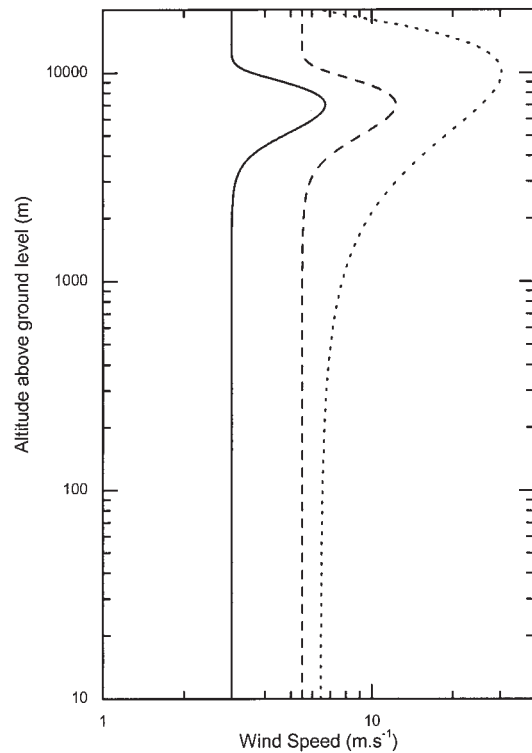


Fig. 2. Horizontal wind speed ( $V$ ) profiles for the MK median (dotted curve), the SP median (dashed curve), and the SP25 (solid curve) atmospheres. The MK wind speed is from the Bufton model. The SP wind speed profiles are analytical fits to SP meteorological balloon data.

Table 1. The ground-level wind speed is the same order of magnitude at SP and at MK. However, the SP upper-atmosphere wind speeds are significantly lower, consistent with the low turbulence observed at high altitudes. The SP high-altitude component peaks at a lower altitude ( $\sim 7$  km) than that of MK ( $\sim 10$  km).

### 3. Wave-Front Errors

For the residual wave-front error (by means of the residual phase variance) after adaptive-optics correction to be estimated, the turbulent wave front  $\phi(r, \alpha)$  from a given source on the sky located at an off-axis angular distance  $\alpha$  is expressed as the polynomial expansion over the telescope of aperture radius  $R$  by

$$\phi(R\rho, \alpha) = \sum_{j=2}^{\infty} a_j(\alpha) Z_j(\rho), \quad (8)$$

where  $\rho$  is the normalized aperture position vector ( $r/R$ ) and the expansion coefficients are given by

$$a_j(\alpha) = \int W(\rho) \phi(R\rho, \alpha) Z_j(\rho) d^2\rho. \quad (9)$$

$W$  is the telescope aperture function (1 for  $r < R$ ; 0 otherwise), and the piston term ( $j = 1$ ) has been neglected because it represents only an average phase variance across the telescope aperture and

thus does not effect the resolution. Various other expansions have been used in the literature to represent wave-front distortions in adaptive optics systems.<sup>33</sup> The Zernike polynomial expansion is used in the current analysis because of its simple analytical expressions. The polynomial terms are given by<sup>34</sup>

$$Z_j = \sqrt{n+1} \begin{cases} R_n^m(\rho) \sqrt{2} \sin(m\theta) & m \neq 0, j_{\text{even}} \\ R_n^m(\rho) \sqrt{2} \cos(m\theta) & m \neq 0, j_{\text{odd}} \\ R_n^0(\rho) & m = 0 \end{cases} \quad (10)$$

where

$$R_n^m = \sum_{s=0}^{(n-m)/2} \frac{(-1)^s (n-s)!}{s! [(n+m)/2 - s]! [(n-m)/2 - s]!} \rho^{n-2s} \quad (11)$$

Tabulations of the residual phase variance after adaptive-optics correction of the first  $j$  Zernike terms have been derived by Noll<sup>34</sup> and Roddier.<sup>35</sup> This variance represents the fitting error that is due to the finite number of actuators across the deformable mirror. It is a good indicator of the adaptive-optics capability for a telescope at a particular site. The variance is found to scale with  $(D/r_0)^{5/3}$  for an increase in the number of modes corrected. Reference 36 gives the residual phase variance for correction of modes up to radial order  $n = N$ , which corresponds to correction up to a polynomial of order  $j$ , where  $N = (j+1)(j+2)/2$ . Considering only radial order modes simplifies the computation. The residual phase variance is given by

$$\Delta\phi_{\text{res}}^2(N) = 3.895 \left(\frac{D}{r_0}\right)^{5/3} \left[ \sum_{n=1}^{\infty} (n+1)^2 I_{n,0}(0) - \sum_{n=1}^N (n+1)^2 I_{n,0}(0) \right], \quad (12)$$

where

$$I_{n,0}(0) = \int_0^{\infty} x^{-14/3} J_{n+1}^2(x) dx \quad (13)$$

and  $J_k$  is the Bessel function of order  $k$ . The first term in brackets in Eq. (12) represents the phase variance introduced by the uncompensated atmosphere [ $1.0299 (D/r_0)^{5/3}$ ]; the second term represents the phase variance of Zernike terms of radial order higher than  $N$ . This radial-order evaluation of the residual phase variance gives good agreement with the values for individual Zernike term variance as tabulated by Noll.<sup>34</sup> An analytical expression for the Bessel function integral, Eq. (13), is given in Ref. 37 in terms of ratios of gamma functions. In Eq. (12), perfect correction of all terms up to order  $N$  is assumed; the equation does not include errors introduced in the wave-front measurement. It is useful

to provide an indication of the efficiency of an adaptive-optics system in terms of the number of modes corrected and the observation wavelength for a particular site with a particular size of telescope.

Knowing the residual phase variance, one can determine the Strehl ratio,  $S$ , that represents the ratio of the maximum on-axis intensity of the corrected stellar profile to the on-axis intensity of the diffraction-limited point-spread function (the Airy pattern). In terms of telescope size and wave-front errors, the Strehl ratio is given by

$$S = \frac{1 - \exp(-\phi^{10/3}/6)}{1 + (D/r_0)^2} + \exp(-\phi^2). \quad (14)$$

The expression given in Eq. (14) was derived by Racine.<sup>38</sup> Similar expressions are given by Parenti and Sasiela.<sup>26</sup> Unlike the expression for the Strehl ratio of the uncompensated atmosphere,  $S = (D/r_0)^{-2}$ , which is used to derive the FWHM of the seeing disk [Eq. (4)] and is valid only for  $(D/r_0) \gg 1$ , and unlike the expression for the Strehl ratio in terms of the phase variance,  $S = \exp(-\Delta\phi^2)$ , which is valid only for  $\Delta\phi^2 \ll 1$ , Eq. (14) is valid for any degree of atmospheric correction and ratio of  $D/r_0$ . It is therefore appropriate even for partial low-order correction of the tip-tilt modes.

For partial adaptive-optics compensation, the profile of a stellar image is not well represented by either a Gaussian or a Moffat atmospheric point-spread function or a Bessel function representative of the telescope point-spread function. Images produced typically consist of a sharp central core with a variable amount of light scattered into a broader halo; see, for example, Ref. 39. Following Roddier *et al.*,<sup>40</sup> the Strehl width, which represents the width of a uniformly illuminated disk with the same total flux and intensity, is therefore a better indication of the efficiency of an adaptive-optics system than the FWHM of the atmospheric point-spread function.

Figure 3 shows the Strehl ratio that is achievable with increasing Zernike mode correction as a function of wavelength. Both 2- and 8-m telescopes are considered with MK, SP, and SP25 atmospheric profiles. As indicated in the figure, low-order adaptive-optics correction is more efficient for the MK atmosphere. This is due entirely to the lower value of  $r_0$ . Perfect tip-tilt correction on a 2-m telescope achieves essentially diffraction-limited imaging (where diffraction limit is defined as a Strehl ratio greater than 0.8)<sup>33</sup> for wavelengths longer than 3.3, 6.7, and 4.6  $\mu\text{m}$  for the MK, SP, and SP25 atmospheres, respectively. High-order correction of the first 10 radial modes gives diffraction-limited imaging at wavelengths above 0.8, 1.6, and 1.1  $\mu\text{m}$ , respectively, for the three atmospheres. As the number of modes corrected for is increased, the efficiency of the correction of the Antarctic telescope increases relative to the MK telescope.

As the telescope diameter is increased, the phase variance for any order of correction increases by the 5/3 power of the diameter [from Eq. (12)]. There-

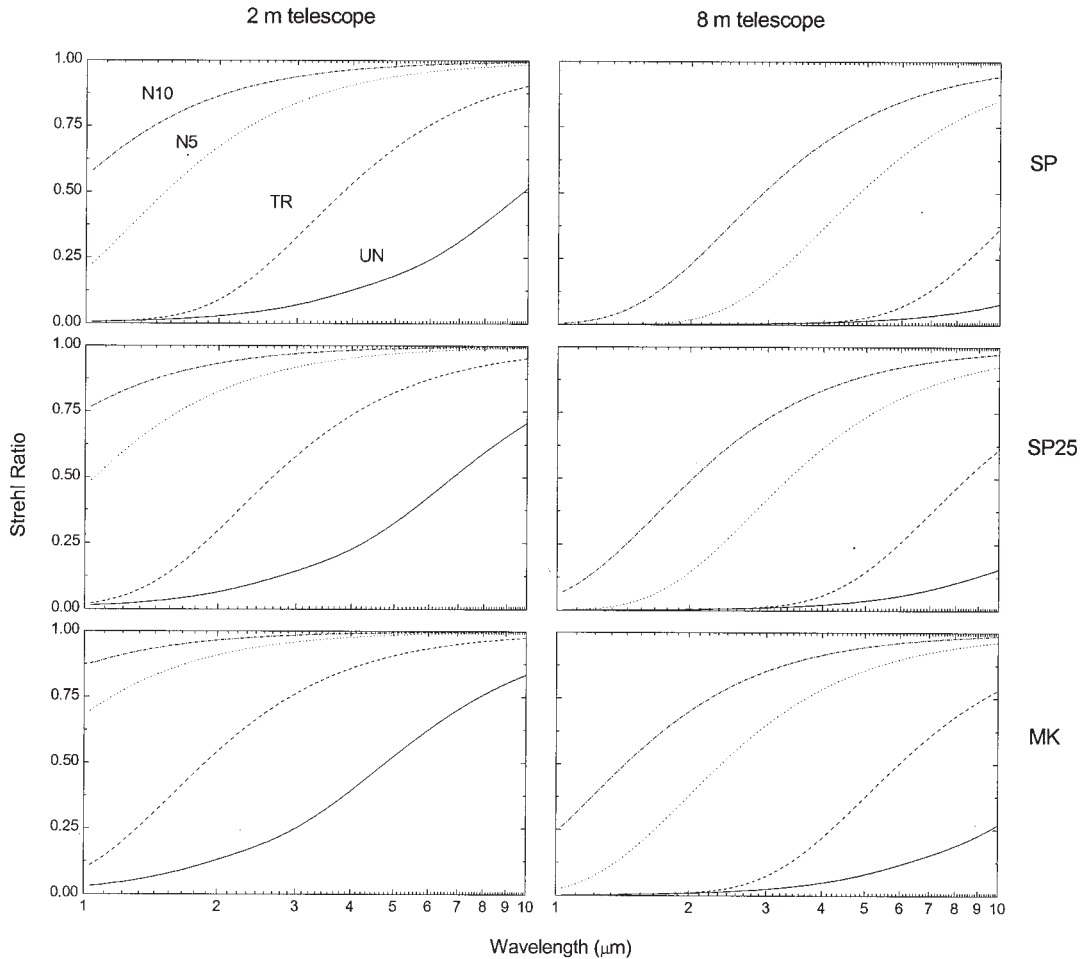


Fig. 3. Strehl ratio achievable with perfect on-axis adaptive-optics correction for a 2-m telescope and an 8-m telescope. The MK atmosphere, the SP25 atmosphere, and the SP atmosphere are graphed in left-right pairs of figures, as labeled. In each figure the Strehl ratio is shown versus wavelength for the uncompensated atmosphere (UN), tip-tilt removed correction (TR), 5-radial order correction (N5), and 10-radial order correction (N10), as marked in the top left figure.

fore, higher modal correction is required on an 8-m telescope to achieve the same resolution as a 2-m telescope. The low order tip-tilt modes still represent the largest contribution to the total wave-front variance, and thus efficient low-order correction must first be achieved before higher-order modes can be corrected. These values of resolution, as calculated from Eq. (12), consist only of errors that have been introduced by incorrect fitting of the wave front. These errors depend only on the number of modes corrected for, i.e., the number of actuators across the deformable mirror. An accurate model of adaptive-optics system performance must consider other errors introduced during measurement and detection. Such errors are discussed in Sections 4 and 5 below.

#### 4. Tip-Tilt Errors

Correction for the  $Z_2$  and  $Z_3$  ( $N = 1$ ) Zernike polynomial terms, which represent an average tilt of the wave-front phase over the pupil aperture, is generally accomplished with a tip-tilt secondary mirror. Such a device is standard for most infrared telescopes designed today. Although it is often not considered

adaptive optics, the tip-tilt correction is a critical component in determining the resolution performance of any telescope, because the tip-tilt modes represent the largest contribution to the total wave-front variance.

Analysis of tip-tilt errors is important because the total tip-tilt error will often determine the limiting resolution for a telescope equipped with high-order adaptive-optics correction (particularly for a laser-guide star system, which requires a natural guide star to compensate for tip-tilt fluctuation), and the anisoplanatic error associated with the tip-tilt correction determines the useful field of view for a telescope equipped only with a tip-tilt mirror. Operation in Antarctica of a telescope equipped with a tilt-tilt mirror is considered feasible and was demonstrated previously with the SPIREX telescope.

An analysis of the errors associated with tip-tilt correction is given in more detail in Refs. 27 and 41; the procedure is outlined here. The residual phase variance after tip-tilt correction can be written as

$$\Delta\phi_{\text{tilt}}^2 = \Delta\phi_{\text{res}}^2 + \phi_{\text{ta}}^2 + \phi_{\text{snr}}^2 + \phi_{\text{bw}}^2 + \phi_{\text{ca}}^2, \quad (15)$$

where the first term of Eq. (15) is the residual tip-tilt phase variance calculated from Eq. (12) (i.e., assuming perfect correction):

$$\Delta\phi_{\text{res}}^2 = 0.134(D/r_0)^{5/3}. \quad (16)$$

The next four terms of Eq. (15) represent tilt anisoplanatic error, SNR error, bandwidth error, and centroid anisoplanatic error, respectively. The following analysis is simplified, and comparison with other work is aided, by expression of the tip-tilt phase variance,  $\phi^2$  [rad<sup>2</sup>], as a single-axis rms tilt error,  $\sigma$  [rad]:

$$\sigma = \left[ \phi^2 \left( \frac{2}{\pi^2} \right) \left( \frac{\lambda}{D} \right)^2 \right]^{1/2}. \quad (17)$$

A number of approximations are given in the literature<sup>25,27,41-43</sup> for the tilt anisoplanatic error,  $\sigma_{\text{ta}}$ . From Olivier *et al.*<sup>27</sup>

$$\sigma_{\text{TA}} = 6.14D^{-1/6} \left\{ [s](\theta) \int_0^\infty C_N^2(z) f_\Delta(z) dz \right\}^{1/2}, \quad (18)$$

where the weighting function  $f_\Delta(z)$  can be approximated by

$$f_\Delta(z) \approx \begin{cases} \frac{8.06 \times 10^{-2} s^{2.04}}{0.513 + s^{1.90}} & s < 40 \\ \frac{0.12 \times 10^{-2} s^{2.04}}{0.511 + s^{1.06}} & s > 40 \end{cases}, \quad (19)$$

$$s = \frac{z\alpha \sec\theta}{D}, \quad (20)$$

where  $\alpha$  is the separation angle between the object and the guide star, and the approximation of the weighting function valid to  $s < 40$  given by Olivier *et al.*<sup>27</sup> has been extended to  $s > 40$  (required because only a 2-m telescope is considered here).

Figure 4 compares the tilt anisoplanatic error calculated from Eq. (18) for a 2-m telescope operated at 2.4  $\mu\text{m}$  with the  $C_N^2$  profile of the MK, SP, and SP25 atmospheres. The function  $f_\Delta(z)$  weights higher components of the atmosphere with higher values as the separation angle,  $\alpha$ , is increased. The error thus increases more rapidly for an atmosphere with high-altitude turbulent contributions (i.e., MK) compared with the SP atmospheres, and hence the SP telescope tilt anisoplanatic error is lower than the MK telescope anisoplanatic error by an order of magnitude. At large separation angles the errors for all atmospheres tend toward similar values. This occurs because the MK tip-tilt contribution approaches the MK uncompensated atmospheric phase variance (4 rad<sup>2</sup>) for such large separation angles.

The SNR tip-tilt error, which arises as a result of

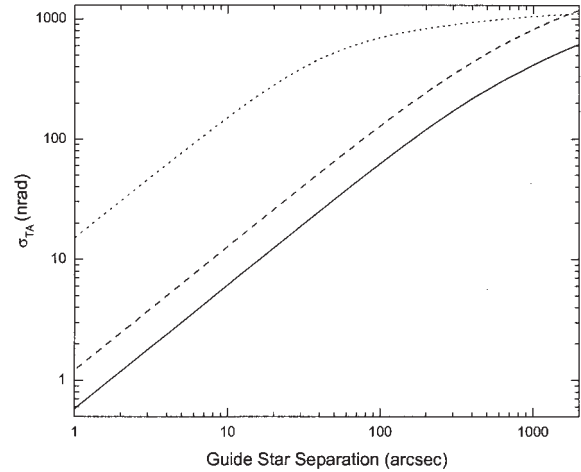


Fig. 4. rms tip-tilt anisoplanatic error for a 2-m telescope operating at 2.4  $\mu\text{m}$  with MK (dotted curve), SP (dashed curve), and SP25 (solid curve) atmospheres as a function of the separation between guide star and object.

the finite SNR in the tip-tilt detection system, is given by<sup>27,41</sup>

$$\sigma_{\text{SNR}} = \frac{3\pi}{16} \frac{\lambda_T}{D} \left[ \frac{2}{\kappa_{tt}} \tan^{-1} \left( \frac{\kappa_{tt}}{2} \right) \right]^{-1/2} \left( \frac{\kappa_{tt} f_c}{\Gamma_0} \right)^{1/2} 10^{m_v/5}, \quad (21)$$

where  $f_c$  is the bandwidth of the feedback loop,  $\kappa_{tt} f_c$  is the sampling frequency of the feedback loop  $\lambda_T$  is the tilt-tilt detection wavelength, and  $\Gamma_0$  is the photon detection rate from a star with zero V-band magnitude,  $m_v$ . Parameters used in the analysis are given in Table 2.

The fourth wave-front error term in Eq. (15) arises from the finite bandwidth of the detection system. There is a temporal delay between the detection of the guide star's wave front and the correction of the object's wave front. Because the wave-front tilt's phase variance is constantly changing, this time delay results in an error in the correction. The error is given by

$$\sigma_{\text{BW}} = \frac{f_T \lambda_T}{f_c D}, \quad (22)$$

where  $f_T$  is the Tyler fundamental tilt tracking frequency,<sup>44</sup> given by

$$f_T = 0.331D^{-1/6} \lambda_T^{-1} \{ \sec(\theta) \int_0^\infty C_N^2(z) V_\omega^2(z) dz \}^{1/2}. \quad (23)$$

The tip-tilt tracking frequency is the atmospheric characteristic frequency defined<sup>44</sup> such that, when the servo loop bandwidth is equal to it, the rms tip-tilt error is equal to the diffraction angle ( $\lambda/D$ ). It represents the speed at which the atmospheric phase variance associated with the tip and tilt terms fluctuates. A tilt detection wavelength  $\lambda_t$  of 0.7  $\mu\text{m}$

**Table 2. Values of Parameters Used in Analysis**

Symbol	Parameter	Value
$\theta$	Zenith observation angle	$0^\circ$
$\kappa_{tt}$	Tip-tilt sampling/bandwidth ratio	10
$\lambda_T$	Tip-tilt compensation wavelength	$0.7 \mu\text{m}$
$T_{tt}$	Tip-tilt system transmission	0.6
$\eta_{tt}$	Tip-tilt sensor quantum efficiency	0.8
$\kappa_{ho}$	High-order sampling/bandwidth ratio	10
$\lambda_{ho}$	High-order sensor wavelength	$0.7 \mu\text{m}$
$T_{ho}$	High-order system transmission	0.6
$\eta_{ho}$	High-order sensor quantum efficiency	0.8
$f_{ws}$	High-order servo cutoff frequency	50 Hz
$C$	High-order servo coefficient	5.2
$d_s$	Subaperture diameter	0.4 m
$N_r$	High-order wave-front sensor read noise	5 electrons

(chosen as a compromise between detector efficiency and guide star flux) gives values of  $f_T = 6.3, 4.1, 1.4$  Hz for the MK, SP, and SP25 atmospheres, respectively. Because of the lower wind speed the tip-tilt phase fluctuation at the SP is much slower than that observed at MK. The error associated with the finite bandwidth measurement is correspondingly lower.

The SNR error is proportional to the feedback loop bandwidth (as a lower bandwidth results in a longer integration time and hence in a higher SNR), and the bandwidth error is inversely proportional to the feedback loop bandwidth (as the atmosphere changes less for a higher bandwidth). Hence a value for the optimum feedback loop bandwidth can be derived<sup>27</sup>:

$$f_c^{opt} = 8 \left[ \frac{f_T r_0}{3\pi D} \Gamma_0^{1/2} \left[ \frac{2}{\kappa_{tt}} \tan^{-1} \left( \frac{\kappa_{tt}}{2} \right) \right]^{-1/4} 10^{-m_v/5} \right]^{2/3} \quad (24)$$

A smaller  $f_T$  and a smaller  $r_0$  give a lower value for the optimum feedback loop bandwidth for the SP atmosphere. For example, observation of a 13 magnitude star at  $0.7 \mu\text{m}$  gives optimum frequencies  $f_c^{opt}$  of 12, 5, and 3 Hz for the MK, SP, and SP25 atmospheres, respectively.

Using the optimum feedback loop bandwidth and values of  $\sigma_{bw}$  and  $\sigma_{SNR}$  determined from Eqs. (21) and (22) yields the combined bandwidth and SNR error for the MK, SP, and SP25 atmospheres shown in Fig. 5. The lower tilt tracking frequency of the Antarctic atmosphere (which reduces the bandwidth error) and the lower Antarctic values of  $r_0$  (which increase the SNR error) relative to the MK atmosphere combine to give total errors that are similar for the two cases. The exact relationship changes slightly with wavelength (owing to the change in  $r_0$  for each case, leading to a lower bandwidth-SNR error for the SP telescope relative to the MK telescope at longer wavelengths.

The fifth instrument error term in Eq. (15) is the centroid anisoplanatic error, which arises because the wave-front sensor measures a variance with contributions from high-order modes (see Brummelaar<sup>45</sup> for a discussion of this error). Correcting the tip-tilt

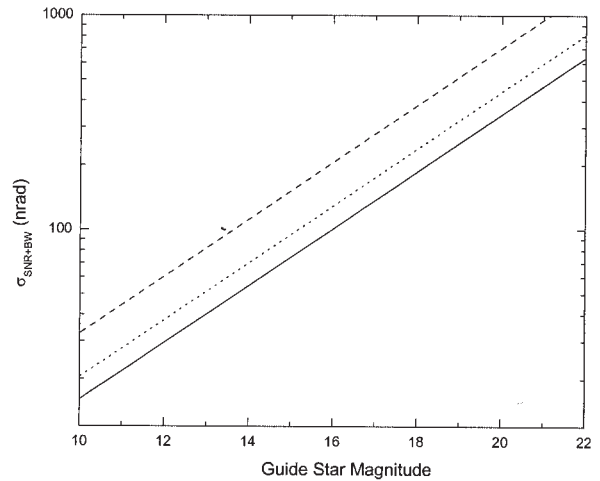


Fig. 5. Combined rms SNR ratio and bandwidth tip-tilt errors as a function of guide star magnitude for a 2-m telescope operating at  $2.4 \mu\text{m}$  with MK (dotted curve), SP (dashed curve), and SP25 (solid curve) atmospheres.

variation for these higher-order modes thus introduces an error. It is given by<sup>41</sup>

$$\sigma_{CA} = (N_c + 1)^{-7/6} 0.00551 \frac{\lambda_T}{D} \left( \frac{D}{r_0} \right)^{5/6}, \quad (25)$$

where  $N_c$  is the number of orders of pure coma (the next highest contribution to the wave-front error) that are measured in the reference wave front. This is often the limiting contribution to the tip-tilt error for low-wavelength ( $<1\text{-}\mu\text{m}$ ) correction, and thus more-sophisticated sensors that are capable of measuring the high-order mode contribution are needed. In the infrared, the other instrumental errors scale with wavelength, whereas this error depends only on the wave-front sensor's wavelength. Thus for infrared correction the centroid error is a negligible factor in the total tip-tilt error, and  $N_c$  is set to 0.

The combined SNR and bandwidth errors increase with the magnitude of the tip-tilt guide star (owing to the decreased SNR). The tilt anisoplanatic error increases with the angular separation of the object and guide stars. As the angular separation increases, the probability of finding a star of brighter magnitude also increases. This probability, which represents the fraction of the sky that has coverage for a given stellar magnitude, is termed the sky coverage factor:

$$P_{sky} = 1 - \exp \left[ -\pi \alpha^2 \sum (m_v, b) \right], \quad (26)$$

where  $b$  is the galactic latitude. It has a different functional form for observations of the galactic plane and the galactic pole. A given sky coverage factor can be represented by a contour in the parameter space of stellar magnitude versus angular separation. These contours are determined from stellar distributions tabulated by Allen<sup>46</sup> and extrapolated to the V band by Olivier and Gavel.<sup>41</sup> For each sky coverage factor a minimum total tip-tilt error can

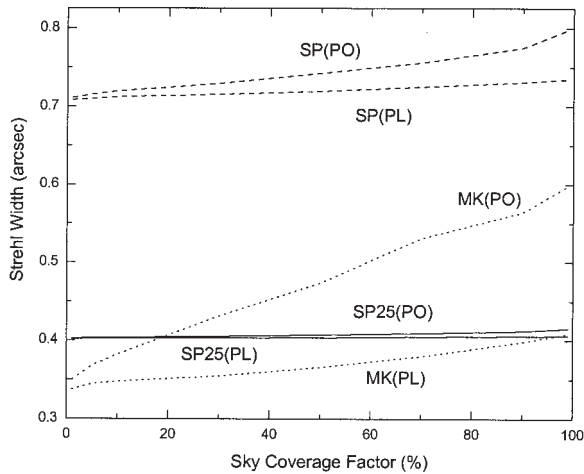


Fig. 6. Strehl width versus sky coverage factor for a 2-m telescope operating at  $2.4 \mu\text{m}$  with tip-tilt correction. The resolution achievable for observations of the galactic plane (PL) and the galactic pole (PO) are shown for the MK, SP, and SP25 atmospheres. The uncompensated atmospheric seeing FWHM at this wavelength is  $0.72''$ ,  $1.46''$ , and  $0.97''$  for the MK, SP, and SP25 atmospheres, respectively. The diffraction-limited telescopic point-spread function FWHM is  $0.25''$ .

thus be determined that represents a particular combination of magnitude and separation (i.e., of SNR-bandwidth error and tilt anisoplanatic error). This total tip-tilt error can then be converted to phase variance from Eq. (17) and to a Strehl ratio from Eq. (14). The Strehl ratio then gives the Strehl width of the partially corrected image.

The Strehl seeing width versus sky coverage factor for an observation wavelength of  $2.4 \mu\text{m}$  with a 2-m telescope is shown in Fig. 6 for each of the MK, SP, and SP25 atmospheres for observation in both the galactic plane and the galactic pole. By virtue of the dense accumulation of stars in the galactic plane, and the superior uncompensated atmospheric seeing, the MK telescope is close to diffraction limited at this wavelength. However, for observations of the galactic pole, the increase in anisoplanatic error for the MK atmosphere dramatically increases the size of the Strehl width. The effect of the low anisoplanatic error for the SP atmosphere is evident from the figure. There is essentially no change in the Strehl width for an increase in sky coverage factor for observations in either the galactic plane or the galactic pole; thus close to 100% of the sky can be observed at the same angular resolution for an Antarctic telescope equipped with tip-tilt correction. This resolution is determined only by the ratio of the on-axis contribution of the tip-tilt term to the uncompensated atmospheric seeing. Although the seeing is considerably less than for the MK telescope for the median SP atmosphere, the best 25% of observations can be made at a seeing size of  $\sim 1.5$  times the diffraction limit.

Figure 7 shows the variation of the Strehl width for a 2-m telescope as a function of wavelength for each atmosphere (MK, SP, SP25) for a sky coverage factor of 90%. In either the galactic plane or the galactic

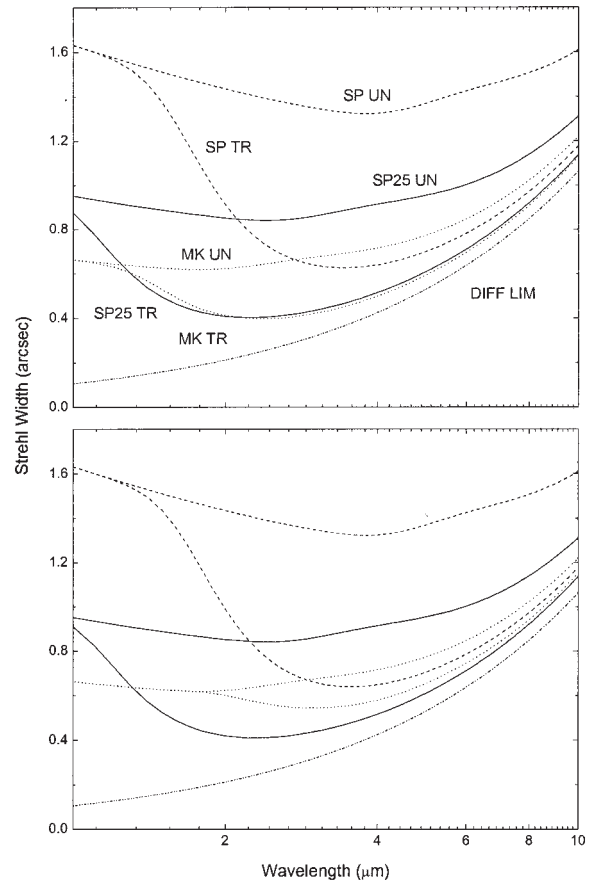


Fig. 7. Strehl width for a 2-m telescope as a function of wavelength for tilt-removed seeing (TR) for MK, SP, and SP25 atmospheres, as marked in the top figure. (a) Observations of the galactic plane, (b) observations of the galactic pole. The Strehl width for each uncompensated atmosphere (UN) and the diffraction limit (DIFF LIM) is also shown in each figure.

pole, the resolution achievable for tip-tilt correction for the SP telescope is determined almost entirely by the higher-order residual error [Eq. (16)], i.e., by the value of  $r_0$ . Because of the large isoplanatic angle, the anisoplanatic errors increase with angular separation at a rate slow enough that very bright stars can always be used, such that the anisoplanatic and SNR errors are negligible compared with the residual error. This is also the case for the MK telescope observing in the galactic plane. For MK observations of the galactic pole, however, the sparse stellar distribution combined with the increased anisoplanatic error gradient results in a minimum error that degrades the resolution because much fainter stars at smaller angular separations have to be used as guide stars. This degradation is such that for observation above  $1.2 \mu\text{m}$  a superior resolution is attainable by the SP telescope for the best 25% of observing conditions.

## 5. High-Order Adaptive-Optics Correction

Similarly as for tip-tilt correction, several measurement and fitting errors are introduced in the correction of high-order modes. Phase variance is caused

by fitting error owing to the presence of residual uncorrected higher-order modes  $\Delta\phi_{\text{res}}$ , by anisoplanatic error owing to the angular separation between the guide star and the object  $\phi_{\text{anis}}$ , by SNR error  $\phi_{\text{SNR}}$ , and by bandwidth error  $\phi_{\text{bw}}$ . The total residual phase variance is then given by

$$\Delta\phi_{\text{ho}}^2 = \Delta\phi_{\text{res}}^2 + \phi_{\text{anis}}^2 + \phi_{\text{SNR}}^2 + \phi_{\text{bw}}^2. \quad (27)$$

The phase variance that is due to the residual fitting error and the anisoplanatic error depends on the number of actuators across the subaperture, i.e., the number of modes corrected and the angular separation. The combined phase variance of these two terms is given by<sup>47</sup>

$$\Delta\phi_{\text{res}}^2 + \phi_{\text{anis}}^2 = 3.895 \left(\frac{D}{r_0}\right)^{5/3} \left\{ \sum_{n=1}^{\infty} (n+1)^2 I_{n,m}(0) - \sum_{n=1}^{\infty} (n+1)^2 [F - I_{n,0}(0)] \right\}, \quad (28)$$

where

$$F = \frac{\int_0^{\infty} C_N^2(z) I_{n,m}(s) dz}{\int_0^{\infty} C_N^2(z) dz}, \quad (29)$$

$$I_{n,m} = \int_0^{\infty} x^{-14/3} J_{n+1}^2(x) J_0(sx) dx - (-1)^m \int_0^{\infty} x^{-14/3} J_{n+1}^2(x) J_{2m}(sx) dx. \quad (30)$$

Function  $F$ , containing integral  $I_{n,m}$ , must be evaluated for each value of the separation angle and for each radial polynomial order.  $I_{n,0}(0)$  is given by Eq. (13), and  $s$  is as defined in Eq. (20). Analytic solutions for the multiple Bessel function integrals in Eq. (30) are derived from Melin transforms and are given in Refs. 37 and 48 in terms of the ratios of gamma functions and hypergeometric series. These functions and series are readily implemented in the Mathematica software package. For the lowest-order (tip-tilt) modes the simpler approximations that were used in Section 4 to derive the tilt anisoplanatic error [Eqs. (18) and (19)] give good agreement with the more-rigorous solutions used here.

Figure 8 compares the residual phase variance and the guide star-object angular separation for the SP and MK atmospheres with an increasing number of radial mode corrections. The units are  $(D/r_0)^{5/3} \text{ rad}^2$ . The total variance thus scales with telescope diameter and the atmospheric value for  $r_0$ . Hence the MK variances are all a factor of  $\sim 4$  smaller for the same telescope size. The figure shows that, for a negligible angular separation, the phase variance reduces to the residual fitting variances given by Noll (i.e., the anisoplanatic error is negligible). As the

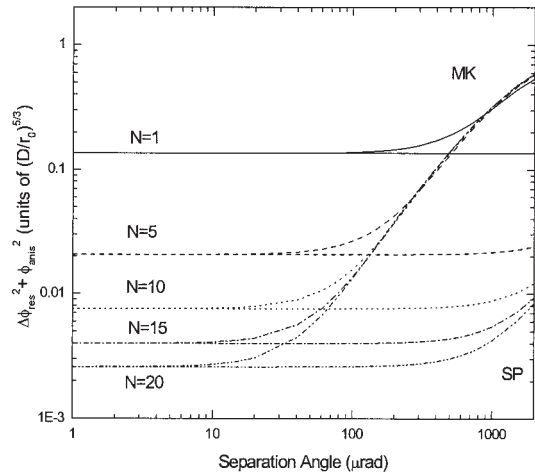


Fig. 8. Residual phase variance from combined residual fitting error and anisoplanatic error versus separation angle between guide star and object for an 8-m telescope with the MK and SP atmospheres. An increasing number of Zernike term corrections (of radial orders  $N = 1, 5, 10, 15, 20$ ) is shown. The units of phase variance are  $(D/r_0)^{5/3} \text{ rad}^2$ . The uncompensated atmosphere introduces a phase variance of 1.0299.

angular separation is increased, the phase variance is constant until it reaches a threshold angular separation above which the anisoplanatic error dramatically dominates the fitting error and until the total variance tends toward the uncompensated atmospheric phase variance. The threshold for the which the anisoplanatic error is lower than the fitting error decreases for an increasing number of modal corrections, as the higher-order modes are spread out over a larger spatial frequency spectrum. Owing to the large higher-altitude contribution to the turbulence found with the MK atmosphere this threshold angular separation is much smaller (by as much as 2 orders of magnitude) than for the SP atmosphere, where the turbulent strength is confined to lower altitudes. The phase variance for the SP25 varies in a similar way to that for the SP atmosphere with wavelength, but the threshold angular separation is larger again for each modal correction.

The anisoplanatic error is related to the isoplanatic angle. The isoplanatic angle is derived from atmospheric moments (path weighted integrals of the refractive-index structure constant) and is given by

$$\alpha_{\text{iso}} = \left[ (2.91) \left( \frac{2\pi}{\lambda} \right)^2 \int_0^{\infty} z^{5/3} C_N^2 dz \right]^{-5/3}. \quad (31)$$

It represents the angular separation for which the Strehl ratio drops to  $1/e$  of its on-axis value, assuming an infinite order of correction; i.e., it does not consider fitting errors or the diameter of the telescope. The anisoplanatic error scales as the  $5/3$  power of the ratio of the angular separation to the isoplanatic angle; this is equivalent to the slope of the combined errors shown in Fig. 8, between the mini-

imum defined by the order of correction and the maximum defined by the uncorrected atmosphere.

The SNR error in the higher-order correction has components that are due to both photon noise and sensor noise.<sup>49,50</sup> It can be described by

$$\phi_{\text{snr}}^2 = \left( \frac{\lambda_{\text{ws}}}{\lambda} \right)^2 \left\{ \frac{4\pi^2 \kappa_{\text{ho}} f_{\text{ho}} [1 + (d_s/r_0)^2]}{3\eta T d_s^2 N_p} + \frac{8\pi^2 N_r^2 \kappa_{\text{ho}}^2 f_{\text{ho}}^2 [1 + (d_s/r_0)^2]}{3(\eta T d_s^2 N_p)^2} \right\}, \quad (32)$$

where  $f_{\text{ho}}$  is the high-order servo bandwidth,  $\kappa_{\text{ho}} f_{\text{ho}}$  is the high-order sampling frequency,  $d_s$  is the subaperture diameter,  $\eta$  is the quantum efficiency of the wave-front sensor detector,  $T$  is the atmospheric and optical system transmission,  $N_r$  is the wave-front sensor's pixel noise,  $\lambda_{\text{ws}}$  is the wavefront sensor's wavelength, and  $N_p$  is the photon density per second from the guide star measured at the wave-front sensor's input. Values for these parameters used in the analysis are given in Table 2.

The phase variance that is due to the bandwidth error has a similar form to the tip-tilt bandwidth error and is given by

$$\phi_{\text{bw}}^2 = C(f_G/f_{\text{ho}})^{5/3}, \quad (33)$$

where  $C$  is a coefficient that depends on the type of servo loop used and  $f_G$  is the Greenwood characteristic atmospheric frequency.<sup>51</sup> The Greenwood frequency, which describes the optimum servo bandwidth for high-order adaptive-optics correction, is given by

$$f_G = \left[ (0.0196) \left( \frac{2\pi}{\lambda} \right)^2 \int_0^\infty v^{5/3} C_N^2(z) dz \right]^{3/5}. \quad (34)$$

The Greenwood frequency is generally an order of magnitude higher than the Tyler frequency for any particular atmospheric profile. This indicates that fluctuations of the higher-order modes occur over a faster time scale than the lower-order tip-tilt fluctuation. As is the case for the Tyler frequency, the SP Greenwood frequency (35 Hz) is significantly lower than the MK Greenwood frequency (50 Hz).

Analogous to the tip-tilt case, increasing the value of the high-order servo bandwidth reduces the variance associated with the bandwidth error and increases the variance associated with the SNR error. Unlike in the tip-tilt case, however, there is no analytical solution to the servo bandwidth that gives a minimum combined variance (owing to the two components of the SNR variance). Although this tends to overestimate the lowest achievable error associated with the SNR and bandwidth terms, a fixed value for the servo loop bandwidth (50 Hz) is used.

The lower value of the coherence length for the SP atmosphere gives a higher variance associated with the SNR measurement, and the lower value of the Greenwood frequency gives a lower variance associated with the bandwidth error. The total combined

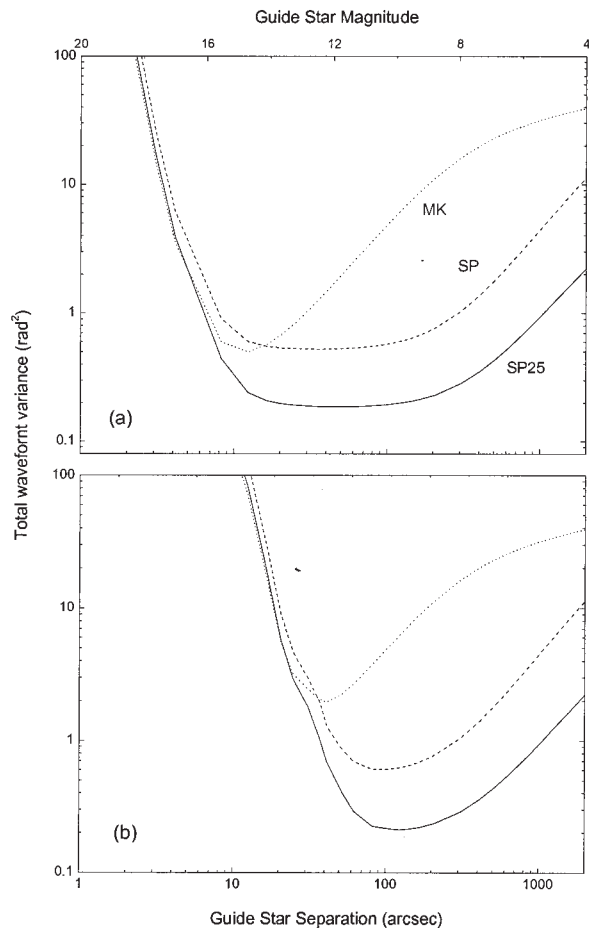


Fig. 9. Total wavefront phase variance versus guide star separation angle and stellar magnitude for sky coverage factors of top, 10% and bottom, 90%. Data are for observations of the galactic plane with an 8-m telescope operated at 2.4  $\mu\text{m}$  with MK, SP, and SP25 atmospheres, as marked in the top figure.

variance for the two atmospheres is thus similar, as was found for the tip-tilt case.

The total wavefront error calculated from Eq. (27) is shown in Fig. 9 for the MK, SP, and SP25 atmospheres relative to guide star separation and magnitude for a 20-radial-mode correction at a wavelength of 2.4  $\mu\text{m}$ . Figure 9(a) shows a 10% sky coverage factor in the galactic plane; i.e., each value of guide star separation corresponds to a probable guide star magnitude. For a 90% sky coverage factor [Fig. 9(b)], also in the galactic plane, each value of guide star separation corresponds to a probable guide star of higher magnitude (i.e., a lower flux). This figure demonstrates the competing error terms. For low angular separations the error is dominated by the SNR error because only faint stars are probable (depending on the sky coverage factor). For large angular separations the SNR error is negligible because much brighter stars can be found; however, the anisoplanatic error is much larger. Because of the rapid increase in anisoplanatic error with angular separation for the MK atmosphere (as indicated in Fig. 8), the minimum error for each sky coverage factor cor-

responds to a small angular separation, which means that the low brightness of the guide star causes the error in SNR to dominate the total error. For the SP telescopes a large separation angle can always be used because of the low anisoplanatic error), which corresponds to bright guide stars with low SNR errors. Thus the total error for the SP telescope is dependent almost entirely on the residual fitting error. The useful field of view is also defined in this figure. For complete sky coverage in the galactic plane the minimum occurs at a guide star separation of  $\sim 200$  arc sec. For galactic pole observations the minimum occurs at a guide star separation of  $\sim 300$  arc sec.

The minimum total variance for each value of sky coverage factor is expressed in Fig. 10 as a Strehl ratio for each atmosphere. Correction for as many as 10 and 20 radial orders is shown. As expected from Fig. 9, the Strehl ratio achievable with the SP system is almost independent of the sky coverage factor. It is also independent of the galactic observation angle, whereas the Strehl ratio achievable with the mid-latitude telescope is strongly degraded for high sky coverage factors and for observations of the galactic pole.

Figure 10 also shows that for the MK atmosphere the number of corrected modes can be reduced to increase the sky coverage factor for a particular observation, i.e., for correction over a wider field of view. This technique is often used<sup>42</sup> at mid-latitude sites. However, it is necessarily accompanied by a reduction in the Strehl ratio (because of the increased residual fitting error). For either SP telescope this technique is not necessary. The low anisoplanatic error, even for high-order modes, indicates that the highest-order correction possible should be used and that this will still give correction over a wide field of view.

The Strehl widths for sky coverage factors of 50% and 90% are shown in Fig. 11 versus wavelength. For each of the MK, SP, and SP25 atmospheres the minimum total phase variance is calculated for each sky coverage factor for each wavelength. Figure 11(a) is for observations in the galactic pole, and Fig. 11(b) is for observations in the galactic plane. For 20-order correction on an 8-m telescope located at the SP, wide-field-of-view ( $>4$ -arc min) diffraction-limited imaging over a large fraction of the sky should be achievable for wavelengths above  $3.5 \mu\text{m}$ , whereas near-diffraction-limited (Strehl ratio,  $>0.5$ ) imaging is possible for wavelengths above  $2.2 \mu\text{m}$ . There is only a small reduction in resolution with an increase in the sky coverage factor. At shorter wavelengths the correction is still significant, and a resolution of  $0.10''$  should be achievable at  $1.2 \mu\text{m}$ . For 25% of the best atmospheric conditions the SP telescope is diffraction limited past  $2.0 \mu\text{m}$  and near diffraction limited past  $1.0 \mu\text{m}$ ; a resolution of  $0.05''$  should be possible at  $1.2 \mu\text{m}$ . The resolution achievable with an adaptive optics system on a MK telescope is better than that achievable on a SP telescope for observations confined to densely populated regions of the

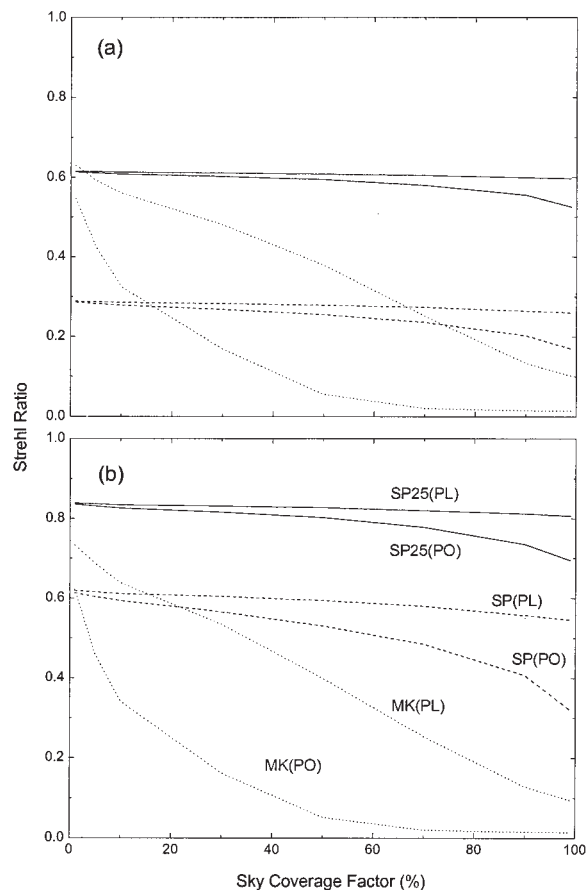


Fig. 10. Strehl ratio versus sky coverage factor for an 8-m telescope operated at  $2.4 \mu\text{m}$  with adaptive optics corrections up to (a) radial order  $N = 10$  and (b) radial order  $N = 20$ . In each figure, galactic plane (PL) and galactic pole (PO) observations are shown for MK, SP, and SP25 atmospheres, as marked in the bottom figure.

galactic plane (less than a few-percent sky coverage factor). However, for an increased sky coverage factor or for observations of the galactic pole MK, high-order adaptive optic systems are ineffective, particularly in the near-infrared and the visible. This drives the necessity for multiconjugate adaptive-optics systems that require multiple laser guide stars at mid-latitude sites.

## 6. Implications

There are many degrees of freedom in a model of the performance of an adaptive-optics system because of the large number of parameters required. Whereas a real system may vary considerably from that presented here, the results distinctly show that, for the same system parameters, Antarctic adaptive-optics systems can achieve significantly superior performance to mid-latitude sites.

The accuracy of the model used here can be determined from comparisons with resolutions reported by actual adaptive-optics systems. Results with the Keck adaptive optics system of Ref. 2 give a seeing size of  $0.044''$  for observations at  $1.65 \mu\text{m}$  from an

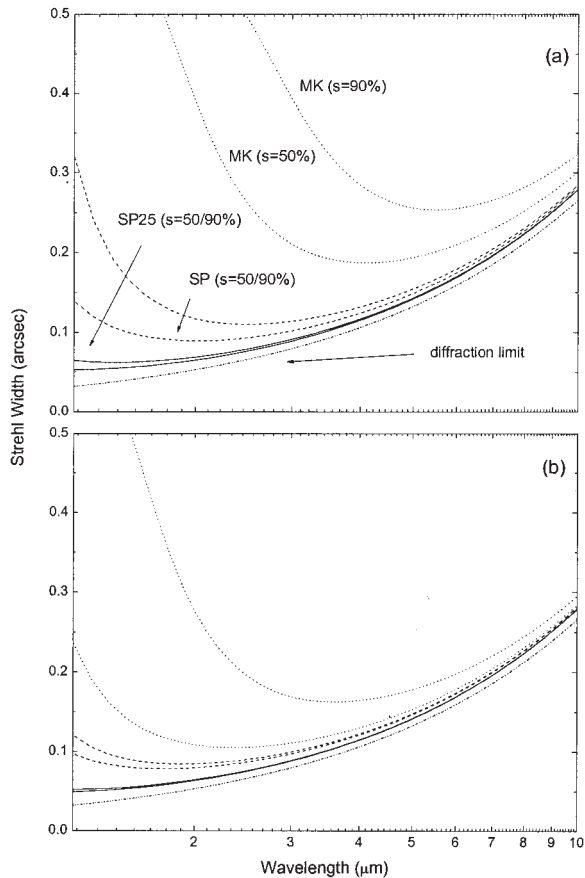


Fig. 11. Strehl width versus wavelength for 20-radial-order Zernike polynomial correction of an 8-m telescope with MK, SP, and SP25 atmospheres, as marked in the top figure. (a) Observations of the galactic pole, (b) observations of the galactic plane. In each case both 50% and 90% sky coverage factors are plotted, as is the diffraction limit.

uncompensated atmosphere of  $0.6''$ . These observations were presumably performed on a source with a bright nearby reference star. Additionally, results from the performance evaluation of the Keck adaptive-optics system<sup>52</sup> demonstrate an achieved *H*-band ( $1.65 \mu\text{m}$ ) resolution of  $0.04\text{--}0.08$  arc sec (depending on the atmospheric conditions). These results are for a range of separation angles ( $15\text{--}30$  arc sec) and *V*-band guide star magnitudes of  $10\text{--}14$ , which represent a maximum galactic-plane sky coverage factor of 1%. The Keck adaptive-optics system consists of a 346-actuator deformable mirror (i.e.,  $\sim 19$  radial-order correction) with a 146-mm clear aperture and a 10-m main mirror diameter. The current model predicts a MK *H*-band resolution of  $0.062''$  for a 10% sky coverage factor in the galactic plane. These results are consistent with those reported, considering the difference in telescope size (8 compared with 10 m) and variability in atmospheric conditions and give confidence to the analysis extended to other wavelengths and telescope sizes.

The motivation for the development of a 2-m telescope for the Antarctic plateau is twofold. First, the telescope is meant as a test bed for future large

optical-infrared telescopes. Second, the low sky background in the near- and mid-infrared indicates that such a telescope would have far superior sensitivity (by as much as 2 orders of magnitude) to any other telescope of similar size located at a good-quality mid-latitude site. Valuable science can therefore be performed on such an instrument. As indicated by Burton *et al.*,<sup>53</sup> one of the primary science goals for a 2-m Antarctic telescope would be to perform near- to far-infrared sky surveys for star formation studies. The design is thus motivated by the requirement for wide-field-of-view imaging capable of covering a large percentage of the galactic plane, with the highest possible resolution for the camera's field of view. A secondary motivation for developing a 2-m Antarctic telescope is to perform wide-field-number count surveys of the galactic pole in the thermal infrared to complement the deep narrow-field surveys that will be conducted by such facilities as the Next Generation Space Telescope. The results presented in this paper indicate that for the median SP atmosphere full sky coverage is possible in the *K* band ( $2.2 \mu\text{m}$ ) with a resolution of  $\sim 0.6''$ , and near-diffraction-limited resolution is achievable longward of the *M* band ( $4.8 \mu\text{m}$ ). A significant improvement was found for the best 25% of observing conditions for which  $\sim 0.4''$  resolution is attainable in the *K* band, and near-diffraction-limited resolution was observed longward of the *L* band ( $3.8 \mu\text{m}$ ). With existing CCD technology a field of view of as much as 30 arc min could be covered at this resolution with a simple focal-plane camera. A significant benefit is obtained because the same resolution is achievable for observations of both the galactic plane and the galactic pole for a SP telescope, whereas for galactic pole observations from mid-latitude sites the percentage of sky covered can be a serious limitation.

The motivation behind the design of an adaptive-optics system on an 8-m telescope must be to achieve the highest resolution possible over the widest field of view. Because of the large anisoplanatic errors that are typical of mid-latitude sites, existing adaptive-optics systems are limited in the fields of view over which they can perform efficient wave-front correction. This represents a serious limitation on the percentage of the sky that can be observed. Although the design of a high-order adaptive-optics system on a large telescope located on the Antarctic plateau would be a serious technological challenge, the benefits in terms of the wide-field-of-view full-sky coverage corrections are significant.

Antarctic sites were previously proposed as appropriate for observations in the infrared for wavelengths longer than  $2.2 \mu\text{m}$ , where the sky's thermal emission dominates the sky's OH emission, and hence the largest increase in sensitivity is found relative to mid-latitude sites.<sup>53</sup> Such observations are suitable for a 2-m tip-tilt telescope, as was mentioned above. However, for high-order adaptive-optics systems operating on much larger telescopes, although a significant relative gain in the achievable resolution

was found at these wavelengths, the largest relative gain (as indicated in Fig. 11) was observed for shorter wavelengths, approaching the visible. This is where mid-latitude sites' adaptive-optics systems have the greatest limitations. Therefore, whereas a large SP telescope with an adaptive-optics system has the highest resolution and sensitivity of any ground-based site in the near- to mid-infrared, it would have comparable sensitivity but superior resolution in the visible to near-infrared.

A site-testing program at the Dome C station is currently being undertaken by the University of New South Wales at the Automated Astrophysical Site-Testing Observatory (AASTINO), which houses the SODAR instrument previously deployed to the SP station. This program has been operating since February 2003. Additionally, a differential image motion monitor (the ADIMM) was operated during summer 2003 at Dome C by the University of Nice. Although a much longer period of data collection is required for a true indication of the site qualities to be obtained, the results can be used as an indication of these qualities. The ADIMM has demonstrated an average seeing of 1.2 arc sec (at 500 nm), and SODAR has demonstrated that the turbulence is mostly confined to 120 m of ground level.

Although few data on the turbulent structure or wind speed profiles for Dome C have been published, one can make a number of assumptions to estimate the performance of a telescope located there. Justifications for believing that Dome C has a distinct (and superior) turbulence profile are discussed in more detail by Marks.<sup>17</sup> Basically, the higher altitude of the site and the topography of the Antarctic continent around the site indicate that the katabatic winds that drive turbulent cells, which originate from the summits of the Antarctic plateau, will never reach the same magnitude at Dome C as at the SP. Satellite observations also indicate that there is rarely a high-altitude jet stream at this location. Summertime measurements of ground wind speed show that it is almost nonexistent ( $\sim 2 \text{ m s}^{-1}$  on average). This is also true in winter. It is thus expected that the Dome C refractive-index structure constant profile will be lower than observed at the SP and will be confined to a region closer to the ground.

Although there is a large uncertainty for any model used, it can be assumed that the Dome C atmospheric profile is at least as good (in terms of astronomical seeing) as the SP atmospheric profile is for the best 25% of time. As has been shown in this paper, a telescope operating with a SP25 atmosphere has significantly superior adaptive-optics capabilities (for both the 2-m tip-tilt and the 8-m high-order systems) to either the SP or the MK atmosphere. This indicates the extraordinary potential of the Concordia Station site.

## 7. Conclusions

Antarctic telescopes with natural guide star adaptive-optics systems have been evaluated. Because of the unique nature of the atmospheric turbu-

lence profile above the Antarctic plateau, anisoplanatic errors associated with the angular separation of guide and object stars are orders of magnitude lower than those found for the turbulence profiles that are characteristic of mid-latitude sites. This finding significantly widens the useful field of view of a high-order adaptive optics system. On an 8-m telescope, near-diffraction-limited observations should be possible at wavelengths longer than  $1.2 \mu\text{m}$  for the best 25% of conditions. Observations at this resolution are possible for close to 100% sky coverage with a wide field of view. These results indicate that telescopes located on the Antarctic plateau do not require multiconjugate adaptive optics systems or multiple laser guide stars.

The author thanks all members of the University of New South Wales Antarctic group for support in this research and in particular John Storey and Michael Burton for valuable comments regarding the manuscript. This research is funded by the Australian Research Council.

## References

1. F. Rigaut, D. Salmon, R. Arsenault, J. Thomas, O. Lai, D. Rouan, J. P. Veran, P. Gigan, D. Crampton, J. M. Fletcher, J. Stilburn, C. Boyer, and P. Jagourel, "Performance of the Canada-France-Hawaii Telescope adaptive optics bonnette," *Publ. Astron. Soc. Pac.* **110**, 152-164 (1998).
2. P. Wizinowich, D. S. Acton, C. Shelton, P. Stomski, J. Gathright, K. Ho, W. Lupton, K. Tsubota, C. Max, J. Brase, J. An, K. Avicola, S. Olivier, D. Gavel, B. Macintosh, A. Chez, and J. Larkin, "First light adaptive optics images from the Keck II telescope: a new era of high angular resolution imagery," *Publ. Astron. Soc. Pac.* **112**, 315-319 (2000).
3. J. M. Beckers, "Adaptive optics for astronomy: principles, performance, and applications," *Annu. Rev. Astron. Astrophys.* **31**, 13-62 (1993).
4. R. I. Davies, W. Hackenberg, T. Ott, A. Eckart, S. Rabien, S. Anders, S. Hippler, M. Kasper, P. Kalas, A. Quirrenbach, and A. Glindemann, "The science potential of ALFA: adaptive optics with natural and laser guide stars," *Astron. Astrophys. Suppl. Ser.* **138**, 345-353 (1999).
5. J. M. Beckers, "Increasing the size of the isoplanatic patch with multiconjugate adaptive optics," in *Proceedings of the European Southern Observatory Conference on Very Large Telescopes and Their Instrumentation*, M. H. Ulrich, ed. (European Southern Observatory, Garching-bei-Muchen, Germany, 1998), pp. 693-703.
6. R. Avila, J. Vernin, and S. Chevas, "Turbulence profile with generalized scidar at San Pedro Martir Observatory and isoplanatic studies," *Publ. Astron. Soc. Pac.* **110**, 1106-1116 (1998).
7. R. D. Marks, J. Vernin, M. Azouit, J. F. Manigault, and C. Clevelin, "Measurement of optical seeing on the high Antarctic plateau," *Astron. Astrophys. Suppl. Ser.* **134**, 161-172 (1999).
8. J. Vernin and C. Munon-Tunoz, "Optical site testing campaign at the Nordic Optical Telescope," *Astron. Astrophys.* **284**, 311-318 (1994).
9. J. W. V. Storey, M. C. B. Ashley, and M. G. Burton, "An automated astrophysical observatory for Antarctica," *Publ. Astron. Soc. Aust.* **13**, 35-40 (1996).
10. J. W. V. Storey, "The AASTO program," in *Astrophysics from Antarctica*, G. Novak and R. H. Landsberg, eds., Vol. 141 of *Astronomical Society of the Pacific Conference Series* (Astronomical Society of the Pacific, San Francisco, Calif., 1998), pp. 313-318.

11. J. S. Lawrence, M. C. B. Ashley, M. G. Burton, P. G. Calisse, J. R. Everett, R. J. Pernic, A. Phillips, and J. W. V. Storey, "Operation of the Near Infrared Sky Monitor at the South Pole," *Publ. Astron. Soc. Aust.* **19**, 328–336 (2001).
12. A. Phillips, M. G. Burton, M. C. B. Ashley, J. W. V. Storey, J. P. Lloyd, D. A. Harper, and J. Bally, "The near infrared sky emission at the South Pole in winter," *Astrophys. J.* **527**, 1009–1022 (1999).
13. M. G. Hidas, M. G. Burton, M. A. Chamberlain, and J. W. V. Storey, "Infrared and submillimetre observing conditions on the Antarctic Plateau," *Publ. Astron. Soc. Aust.* **17**, 260–269 (2000).
14. T. Travouillon, M. C. B. Ashey, M. G. Burton, J. W. V. Storey, and R. F. Lowenstein, "Atmospheric turbulence at the South Pole and its implications for astronomy," *Astron. Astrophys.* **400**, 1163–1172 (2002).
15. A. A. Stark, J. Bally, S. P. Balm, T. M. Bania, A. D. Bolatto, R. A. Chamberlain, G. Engargiola, M. Huang, J. G. Ingalls, K. Jacobs, J. M. Jackson, J. W. Kooi, A. P. Lane, K. Y. Lo, R. D. Marks, C. L. Martin, D. Mumma, R. Ojha, R. Scheider, J. Staguhn, J. Stutzki, C. W. Walker, R. W. Wilson, G. A. Wright, Z. Zhang, P. Zimmerman, and R. Zimmerman, "The Antarctic submillimetre telescope and remote observatory (AST/RO)," *Publ. Astron. Soc. Pac.* **113**, 567–585 (2001).
16. M. Herald, "SPIREX—near infrared astronomy from the South Pole," *Exp. Astron.* **3**, 87–91 (1994).
17. R. D. Marks, "Astronomical seeing from the summits of the Antarctic plateau," *Astron. Astrophys.* **385**, 328–336 (2002).
18. W. J. Wilde, E. J. Kibblewhite, and D. A. Haper, "Performance estimates for a near infrared adaptive optics system at the South Pole," in *Astrophysics from Antarctica*, G. Novak and R. H. Landsberg, eds., Vol. 141 of *Astronomical Society of the Pacific Conference Series* (Astronomy Society of the Pacific, San Francisco, Calif., 1998), pp. 303–310.
19. D. L. Fried, "Optical resolution through a randomly inhomogeneous medium for very long and very short exposures," *J. Opt. Soc. Am.* **56**, 1372–1379 (1966).
20. E. Masciadri and J. Vernin, "Optical technique for inner-scale measurement—possible astronomical applications," *Appl. Opt.* **36**, 1320–1327 (1997).
21. T. S. McKechnie, "Atmospheric turbulence and the resolution limits of large ground-based telescopes," *J. Opt. Soc. Am. A* **9**, 1937–1954 (1992).
22. C. E. Coulman, J. Vernin, Y. Coqueugniot, and J. L. Caccia, "Outer scale of turbulence appropriate to modeling refractive index structure profiles," *Appl. Opt.* **27**, 155–160 (1988).
23. D. L. Fried, "Statistics of a geometric representation of a wavefront distortion," *J. Opt. Soc. Am.* **55**, 1427–1435 (1965).
24. P. Dierickx, "Optical performance of large ground-based telescopes," *J. Mod. Opt.* **39**, 569–588 (1992).
25. G. Valley, "Isoplanatic degradation of tilt correction and short-term imaging systems," *Appl. Opt.* **19**, 574–577 (1980).
26. R. R. Parenti and R. J. Sasiela, "Laser-guide-star systems for astronomical applications," *J. Opt. Soc. Am. A* **11**, 288–297 (1994).
27. S. S. Olivier, C. E. Max, D. T. Gavel, and J. M. Brase, "Tip-tilt compensation: resolution limits for ground-based telescopes using laser guide star adaptive optics," *Astrophys. J.* **407**, 428–439 (1993).
28. B. M. Welsh and C. S. Gardner, "Effects of turbulence induced anisoplanatism on the imaging performance of adaptive-astronomical telescopes using laser guide stars," *J. Opt. Soc. Am. A* **8**, 69–79 (1991).
29. J. L. Bufton, "Comparison of vertical profile turbulence structure with stellar observations," *Appl. Opt.* **12**, 1785–1793 (1973).
30. R. D. Marks, J. Vernin, M. Azouit, J. W. Briggs, M. G. Burton, M. C. B. Ashley, and J. F. Manigault, "Antarctic site testing—microthermal measurements of surface-layer seeing at the South Pole," *Astron. Astrophys. Suppl. Ser.* **118**, 385–390 (1996).
31. J. P. Lloyd, B. R. Oppenheimer, and J. R. Graham, "The potential of differential astrometric interferometry from the high Antarctic plateau," *Publ. Astron. Soc. Aust.* **19**, 318–322 (2002).
32. T. Travouillon, M. C. B. Ashey, M. G. Burton, and J. W. V. Storey, "Seeing measurements at the South Pole using a Hartmann wavefront sensor: ADIMM," *Astron. Astrophys.* (to be published).
33. F. Roddier, "The problematic of adaptive optics design," in *Adaptive Optics for Astronomy*, D. M. Alloin and J. M. Mariotti eds. (Kluwer Academic, Dordrecht, The Netherlands, 1993), pp. 89–111.
34. R. J. Noll, "Zernike polynomials and atmospheric turbulence," *J. Opt. Soc. Am.* **66**, 207–211 (1976).
35. N. Roddier, "Atmospheric wavefront simulation using Zernike polynomials," *Opt. Eng.* **29**, 1174–1180 (1990).
36. G. Molodij and J. Rayrole, "Performance analysis for THEMIS image stabilizer optical system. II. Anisoplanatism limitations," *Astron. Astrophys. Suppl. Ser.* **128**, 229–244 (1997).
37. P. H. Hu, J. Stone, and T. Stanley, "Application of Zernike polynomials to atmospheric propagation problems," *J. Opt. Soc. Am. A* **6**, 1595–1608 (1989).
38. R. Racine, "The telescopic point-spread function," *Publ. Astron. Soc. Pac.* **108**, 699–705 (1996).
39. S. Harder and A. Chelli, "Estimating the point spread function of the adaptive optics system ADONIS using the wavefront sensor measurements," *Astron. Astrophys. Suppl. Ser.* **142**, 119–135 (2000).
40. F. Roddier, M. Northcott, and J. E. Graves, "A simple low-order adaptive optics system for near-infrared applications," *Publ. Astron. Soc. Pac.* **103**, 131–149 (1991).
41. S. S. Olivier and D. T. Gavel, "Tip-tilt compensation for astronomical imaging," *J. Opt. Soc. Am. A* **11**, 368–378 (1994).
42. F. Rigaut and E. Gendron, "Laser guide star in adaptive optics: the tilt determination problem," *Astron. Astrophys.* **261**, 677–684 (1992).
43. D. P. Greenwood and R. R. Parenti, "Synthetic beacons for atmospheric compensation," in *Adaptive Optics for Astronomy*, D. M. Alloin and J. M. Mariotti, eds. (Kluwer Academic, Dordrecht, The Netherlands, 1993), pp. 185–204.
44. G. A. Tyler, "Bandwidth considerations for tracking through turbulence," *J. Opt. Soc. Am. A* **11**, 358–367 (1994).
45. T. A. ten Brummelaar, "The contribution of high order Zernike modes to wavefront tilt," *Opt. Commun.* **115**, 417–424 (1995).
46. C. W. Allen, *Astrophysical Quantities* (Athlone, London, 1976).
47. J. Stone, P. H. Hu, S. P. Mills, and S. Ma, "Anisoplanatic effects in finite-aperture optical systems," *J. Opt. Soc. Am. A* **11**, 347–357 (1994).
48. G. Molodij and G. Rousset, "Angular correlation of Zernike polynomials for a laser guide star in adaptive optics," *J. Opt. Soc. Am. A* **14**, 1949–1965 (1997).
49. G. A. Tyler and D. L. Fried, "Image-position error associated with a quadrant detector," *J. Opt. Soc. Am. A* **72**, 804–809 (1982).
50. R. W. Wilson and C. R. Jenkins, "Adaptive optics for astronomy: theoretical performance and limitations," *Mon. Not. R. Astron. Soc.* **268**, 39–61 (1996).
51. D. P. Greenwood, "Bandwidth specification for adaptive optics systems," *J. Opt. Soc. Am.* **67**, 390–392 (1977).
52. P. Wizinowich, W. M. Keck Observatory Adaptive Optics Home Page (2000): <http://www2.keck.hawaii.edu:3636/inst/ao/ao.html>.
53. M. G. Burton, J. W. V. Storey, and M. C. B. Ashley, "Science goals for an Antarctic Large Infrared Telescope," *Publ. Astron. Soc. Aust.* **18**, 158–165 (2001).